Heliyon 5 (2019) e02409

Contents lists available at ScienceDirect

Heliyon

www.elsevier.com/locate/heliyon

The transition state conformational effect on the activation energy of ethyl acetate neutral hydrolysis

Febdian Rusydi [a,b,c,*], Nufida D. Aisyah [b,d], Rizka N. Fadilla [b,d], Hermawan K. Dipojono [d], Faozan Ahmad [e], Mudasir [f], Ira Puspitasari [b,g], Andrivo Rusydi [h]

[a] Department of Physics, Faculty of Science and Technology, Universitas Airlangga, Jl. Mulyorejo, Surabaya 60115, Indonesia
[b] Research Center for Quantum Engineering Design, Faculty of Science and Technology, Universitas Airlangga, Jl. Mulyorejo, Surabaya 60115, Indonesia
[c] Visiting Researcher at Precision Sciences & Technology and Applied Physics, Graduate School of Engineering, Osaka University, Suita 565-0871, Japan
[d] Department of Engineering Physics, Faculty of Industrial Engineering, Institut Teknologi Bandung, Bandung 40132, Indonesia
[e] Department of Physics, Faculty of Mathematics and Science, Institut Pertanian Bogor, Bogor 16680, Indonesia
[f] Department of Chemistry, Faculty of Mathematics and Science, Universitas Gadjah Mada, Yogyakarta 55281, Indonesia
[g] Information System Study Program, Faculty of Science and Technology, Universitas Airlangga, Jl. Mulyorejo, Surabaya 60115, Indonesia
[h] Department of Physics, Faculty of Science, National University of Singapore, Singapore 117542, Singapore

ARTICLE INFO

Keywords:
Organic chemistry
Physical chemistry
Theoretical chemistry
Long-range correction
First-principles calculations
Neutral hydrolysis
Ester
Density functional theory
Ethyl acetate
Activation energy
Conformational effect

ABSTRACT

We report a first-principles study on ethyl acetate neutral hydrolysis in which we focus on the activation energy variation resulting from the conformational effect in the transition state. We use the conformers of ethyl formate, ethyl acetate, ethyl fluoroacetate, and ethyl chloroacetate as the ester models and one water molecule with a one-step reaction mechanism. We also consider the long-range interaction and the surrounding water in the form of PCM. Our results show that the various conformers yield a significant range of activation energy. Moreover, the gauche conformer has lower activation energy than the trans conformer. The activation energy in its own right is lowered by the halogen atoms. Finally, we remark that the long-range correction and PCM stabilize the transition state geometry but raise the activation energy.

1. Introduction

It is commonly known that neutral hydrolysis of an ester is generally slow. For instance, the rate constants (in 1/s) of methyl acetate and ethyl acetate are an order of 10^{-9} [1] and 10^{-10} [2] respectively. An ester (R–CO_2–R′) with a long chain also has low rate constant such as achetylcholine [R=CH_3, R′=$C_2H_4N^+(CH_3)_3$] with a rate constant of an order of 10^{-9} [3]. The rate constant is higher when halogenated substitution is introduced to the ester. For instance, the alkyl- and aryl-substituted trifluoroacetates (with R′=C_nH_{2n+1}, $n = 3$, 4, and 5) has an order of 10^{-6} [4], chloromethyl chloroacetate has an order of 10^{-5} [5], while ethyl trifluorothiolacetate ($CF_3COSC_2H_5$) has a rate constant with an order of 10^{-3} [6].

Even though it is slow, the neutral hydrolysis is part of the measured rate constant. The measured rate constant, k_m, is

$$k_m = k_0 + k_a + k_b$$

where the first term is the rate constant of neutral hydrolysis and the last two terms are the rate constant of the acid- and base-induced hydrolysis, respectively. Since k_0 is experimentally difficult to obtain, it is common to apply some extrapolation technique [7]. Following an argument presented by Wolfenden and Yuan [3], neutral hydrolysis of an ester might emerge as the predominant factor at an elevated temperature. If it is the case, neutral hydrolysis cannot be ignored and becomes important, especially when one is interested to study biochemistry based on the achetylcholine hydrolysis.

However, the mechanism of neutral hydrolysis of an ester is not fully understood [8] and its theoretical study is very limited [9]. One way to respond to this challenge is by using a computational approach where a reaction is modeled and studied under first-principles calculations. A common modeling approach is to involve water molecules that act as

* Corresponding author at: Department of Physics, Faculty of Science and Technology, Universitas Airlangga, Jl. Mulyorejo, Surabaya 60115, Indonesia.
E-mail address: rusydi@fst.unair.ac.id (F. Rusydi).

https://doi.org/10.1016/j.heliyon.2019.e02409
Received 20 December 2018; Received in revised form 12 August 2019; Accepted 29 August 2019

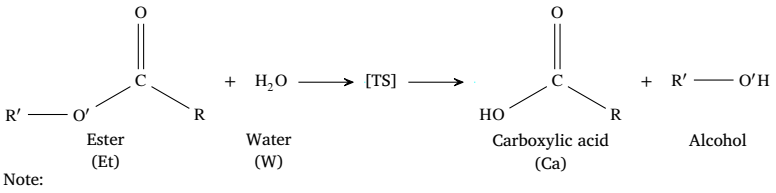

Note:

(i) Isolated reactant is state **1a**; Transition State (TS) is state **1b**; isolated product is state **1c**.
(ii) Abbreviation Et, W, and Ca are used as molecule names throughout the manuscript.

Scheme 1. The one-step reaction model in this study.

Table 1
Selected ester models based on Scheme 1. The R′-group is always C_2H_5.

R	Ester (Label)		Reaction product
H	Ethyl formate	(Et1)	Ca1 + Ethanol
CH_3	Ethyl acetate	(Et2)	Ca2 + Ethanol
CH_2F	Ethyl fluoroacetate	(Et3)	Ca3 + Ethanol
CH_2Cl	Ethyl chloroacetate	(Et4)	Ca4 + Ethanol

a bifunctional acid-base catalyst [10, 11, 12, 13], to model the aqueous as a reaction field [14, 15], or to combine both methods [8, 16].

The study of neutral hydrolysis of an ester becomes interesting. It can be a model for acomputational study of the cholinergic hypothesis. The hypothesis involves the depletion of acetylcholine molecules that may lead to Alzheimer's disease [17, 18]. Acetylcholine belongs to the ester family and has conformers [19, 20, 21, 22, 23]. The conformation affects its stability and activity [24, 25, 26, 27].

In this article, we report our finding on the conformational effect of the ester neutral hydrolysis. All aforementioned theoretical studies showed the importance of a transition state, but none has explored the different arrangement of atoms in the transition states. It is because most theoretical studies so far concern on the methyl acetate family as the ester models, hence no conformer in the transition state. A conformer is likely to exist in an ester with an R or R′ group that has two or more C atoms, such as ethyl acetate. There are two previous works on ethyl acetate (the trans conformer) neutral hydrolysis, which are reported by Schmeer and Sturm [12] and Yamabe et al. [14]. The former used two H_2O molecules, one of which served as the nucleophilic reagent and the other as the acid-base catalyst, and was calculated with Hatree-Fock method. The later used one H_2O molecule and considered Onsager's model as the water surrounding and was calculated with density functional theory method. However, no conformational effect has been reported. To see the variation of conformational effect, we study conformers of four molecule from the ethyl acetate family: ethyl formate, ethyl acetate, ethyl fluoroacetate, and ethyl chloroacetate as the ester models. We also consider the long-range interaction and surrounding water as solvent effect.

2. Methods

Reaction model. We carry out the one-step mechanism to model the neutral hydrolysis as shown in Scheme 1. We use four ester models as listed in Table 1 and notations in Table 2.

The one-step mechanism is argued by Shi et al. [9] as favored if tetrahedal intermediates have a short lifetime and do not interconvert prior to breakdown. The one-step mechanism ensures one saddle point between an initial state (**1a**) and a final state (**1c**) since our concern is on the conformational effect at the saddle point (transition state, **1b**). As da Silva et al. [8] reported, the usual method for searching state **1b** may not work for this kind of study; therefore, we take a great care in ensuring that the saddle point is computationally correct.

DFT calculations. We perform the ground state calculation routines on the basis of density functional theory (DFT) [28, 29] and 6-311++G(d,p) basis set that are integrated into the Gaussian 09 software

Table 2
List of notations used throughout the manuscript.

Notation	Meaning
XC1g	B3LYP (gas phase)
XC2g	CAM-B3LYP (gas phase)
XC1s	B3LYP coupled with PCM (solvent)
XC2s	CAM-B3LYP coupled with PCM (solvent)
R(X,Y)	Bond length between X and Y atom (in Å)
A(X, Y, Z)	$\angle XYZ$ (in degree)
Expr.	Experimental value in gas phase
err._{n0}	(XC*n*g − Expr.)/Expr. (in %)
err._{nsg}	(XC*n*s − XC*n*g)/XC*n*g (in %), $n = 1, 2$
err._{21}	(XC2g − XC1g)/XC1g (in %)
Δ_{21}	XC2g − XC1g
Δ_{sg}	XC*n*s − XC*n*g, $n = 1, 2$
range	maximum − minimum value
rat._{21}	XC2g/XC1g
rat._{nsg}	XC*n*s/XC*n*g, $n = 1, 2$
rat._{k}	ratio of maximum and minimum $k(T)$

[30]. For the exchange-correlation functional, we employ B3LYP [31] and CAM-B3LYP [32] which have been integrated into the software as well. The former has provided good prediction in our previous studies on molecular orbital interaction problems [33, 34, 35, 36], excitation in solvent problems [37, 38], and reaction path coordinate to calculate the tunneling probability [39, 40, 41]. Meanwhile, the latter is needed to consider the correction of the long-range interaction in states **1a**, **1b**, and **1c**. We consider the surrounding water as a perturbation to the systems of interest such that we can couple the DFT calculation with the polarized continuum model (PCM) calculation [42], which is also integrated into the software. We use notations in Table 2 to simplify the writing of the exchange-correlation functionals and PCM coupling calculations.

The Transition State Searching. We set up four steps, with the first three aiming to determine the correct geometry of [Et–W] complex in the transition state (state **1b** in Scheme 1). Step one is to determine the electrophilic site where the water molecule may attack. We analyze the charge population by using NBO program [43] which is integrated into the Gaussian 09 software. Step two is to calculate the potential energy surface (PES) in the plane where the electrophilic site lies (see Fig. 1a). This is done by using partial optimization calculations where the distance of oxygen atom of water and the electrophilic site is fixed. The PES result provides a guide to construct the geometry of TS which becomes the input for step three: to perform TS optimization to predict the geometry of **1b**, which is then followed by the intrinsic reaction coordinate (IRC) calculations. The correct TS geometries require one imaginary frequency to indicate that they are in the saddle point. Step four is to optimize the geometries at two minima predicted by IRC calculations to confirm the molecular geometry in state **1a** and **1c**.

We perform the first three steps with XC1g. Once the geometry of transition state is determined (see Fig. 1b), we repeat step 3 and 4 with XC2g, XC1s, and XC2s.

Possible Transition State Conformers. Fig. 1–3 show the nomenclature we use throughout the manuscript. There are two configurations to form a conformer. First is the R′ part of the ester: C3 position with respect

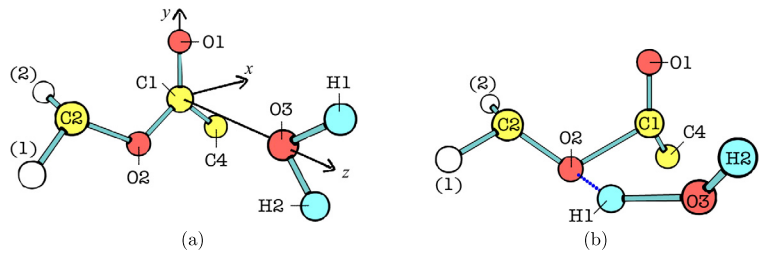

Fig. 1. Molecular model of [Et – W] complex: (a) Initial position of H_2O for the potential energy surface calculation to form the complex , C1–O3 distance is 3.00 Å. (b) The typical optimized geometry of the complex in the transition state. Atom C3 may be positioned at (1) trans or (2) gauche.

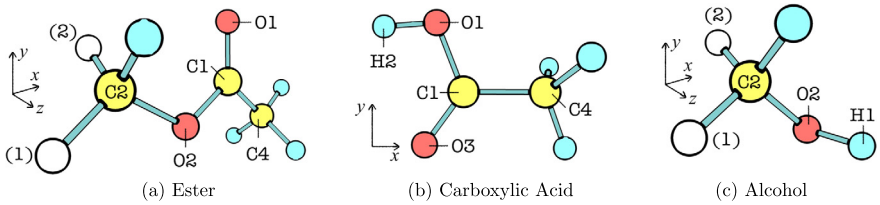

Fig. 2. Illustration of (a) ester, (b) carboxylic acid, and (c) alcohol for nomenclature used throughout the manuscript. Label (1) is for trans and (2) is for gauche conformation with respect to the position of C3. One H atom bound to C2 and three H atoms bound to C4 are shown to give the illustration the correct perspective.

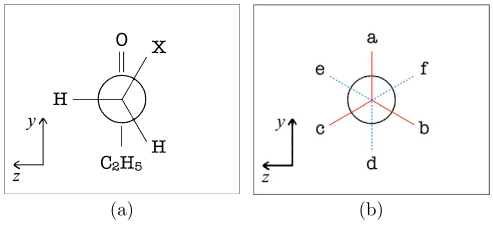

Fig. 3. (a) Newman projection along C1–C4 bond. The "X" is the position of H atom in Et2 and of halogen atom in Et3 and Et4. (b) The eclipse conformation is defined when "X" is at "a", "b", or "c"; while in staggered ones are at "d", "e", or "f".

to C2–O1–C1 plane, which are (1) trans and (2) gauche (Fig. 1 and 2). Second is the R part of the ester: Orientation of "X" with respect to O (Fig. 3) which gives eclipsed ("a", "b", or "c") and staggered ("d", "e", or "f"). Based on these two configurations, we construct conformers of [Et–W] complex at state **1b**, along with their corresponding molecules at state **1a** and **1c**.

For simplicity, we use the following notation "molecule label(R′ – R configuration)". For examples: Et2(1-a) is ethyl acetate with a trans R′ and a staggered R conformation; Ct2(2) is acetic acid with a gauche conformation , Et3(2-d) is ethyl fluoroacetate with a gauche R′ and an eclipsed R conformation where F atom is at "d".

Chemical Kinetic Calculations. Our interest quantity is the activation energy. The activation energy is expressed in term of the standard Gibbs activation energy, $\Delta^{\ddagger}G^{\circ}$ that is the total energy difference between state **1b** and **1a**. The total energy of a state is the total electronic energy with a correction from Gibbs free energy. The former is the results of DFT calculations while the latter is the results of force constant calculations which is integrated into the software. We extend the usefulness of $\Delta^{\ddagger}G^{\circ}$ to calculate the rate constant $k(T)$ based on the transition-state theory [44],

$$k(T) = \frac{k_B T}{h c^{\circ}} \exp\left[\frac{\Delta^{\ddagger}G^{\circ}}{RT}\right] \quad (1)$$

with k_B, h, R are the constant of Boltzmann, Planck, and molar gas, c° is the molecule's concentration from the reactant to the transition state (which we assume to be 1), and T is the temperature (which we assume to be the room temperature, 298.15 K).

3. Results and discussion

3.1. On the ground state structures

The effect of long-range correction. We use Et2(1-a), W, Ca2(1), and ethanol to investigate the effect of the long-range correction on their ground state structures. The reason is that these molecules are experimentally well studied.

Table 3 resumes geometrical parameters from the experiment and our DFT calculations (gas phase). The important value here is the percentage error with respect to the experimental value (err.). The error in general is about less than 1% which corresponds to an order of 10^{-3} Å or 0.1°. This implies both exchange-correlation functionals are excellent to study the ground state structures of the molecules of interest.

Table 4 lists the charge population at some selected atoms. The number of charges does not change significantly after the long-range correction is applied to the calculation. Since the charge population is directly related to the electronic structures of the molecule, the long-range correction does not significantly change the geometrical and electronic structures of the molecule of interest. Therefore, we can conclude that the electrophilic site clearly is at C1 for all exchange correlation functional cases. A water molecule, which has a nucleophilic site at its O3 atom, favorably attacks C1 atom. This makes the starting point of the hydrolysis mechanism shares similarity with that of base-induced ester hydrolysis (Fig. 1a). This analysis becomes our bases on selecting the PES calculation, which we carry in yz-plane where O1, C1, and O3 atoms lie. Fig. 4 shows the PES calculations where the expected entrance of water molecule is at $(z, y) = (1.0, 0.0)$ and it has the highest barrier.

We also present the charge population at C1 and C4 for all esters in Table 5. These two atoms are close to halogen atom in Et3 and Et4. The long-range correction does not change significantly for the charge population at C4, but it does at C1 in Et3 molecules. The Δ_{21}(C1) average is 0.033 e hence it makes the trend linear: the heavier halogen atom at C4, the more negative the C1 and the more positive the C4. This trend is understandable by considering that (1) the electronegativity of F and Cl (Et3 and Et4, respectively) is higher than C (Et2) and (2) the valence electrons of F is 2p while those of Cl is 3p.

The significant difference between XC1g and XC2g is the calculated total electronic energy (E). Fig. 5 shows the energy level diagram of four molecules in Table 3. The diagrams clearly show that the long-range correction consistently increases E. Except water (Fig. 5b), E increases more than 2 eV; it is almost 4 eV in the case of Et2 (Fig. 5a).

Table 3
Selected geometrical parameters of ethyl acetate, water, acetic acid, and ethanol in the ground state.

Parameter	Expr.	DFT				DFT + PCM			
		XC1g	err.$_{10}$	XC2g	err.$_{20}$	XC1s	err.$_{sg}$	XC2s	err.$_{sg}$
(a) Ethyl acetate, Et2(1-a) (Expr. from [46])									
R(C1,C4)	1.508	1.508	0.0	1.501	−0.5	1.505	−0.2	1.498	−0.2
R(C1,O1)	1.203	1.207	0.3	1.203	0.0	1.214	0.6	1.210	0.6
R(C1,O2)	1.345	1.351	0.5	1.343	0.2	1.343	−0.6	1.335	−0.6
R(C2,C3)	1.515	1.515	0.0	1.509	0.4	1.514	−0.1	1.508	−0.1
R(O2,C2)	1.448	1.450	0.1	1.440	−0.6	1.456	0.4	1.445	0.4
A(O1,C1,C4)	125.4	125.5	0.1	125.5	0.1	125.3	−0.2	125.3	−0.2
A(C4,C1,O2)	110.8	111.0	0.2	111.3	0.4	111.5	0.4	111.7	0.4
A(C3,C2,O2)	123.8	123.4	−0.3	123.2	−0.5	123.3	−0.1	123.0	−0.1
A(O2,C2,C3)	108.2	107.6	−0.5	107.6	−0.6	107.6	0.0	107.6	0.0
A(C1,O2,C2)	117.3	116.6	−0.6	116.5	−0.7	117.4	0.7	117.3	0.7
(b) Water (Expr. from [45])									
R(O3,H)	0.958	0.962	0.5	0.960	0.3	0.964	0.2	0.962	0.2
A(H1,O3,H2)	104.5	105.0	0.5	105.5	0.9	104.5	−0.5	104.9	−0.6
(c) Acetic acid, Ca2(1) (Expr. from [45])									
R(C1,C4)	1.520	1.504	−1.1	1.498	−1.5	1.501	−0.2	1.495	−0.2
R(C1,O3)	1.214	1.205	−0.7	1.200	−1.1	1.212	0.5	1.207	0.6
R(C1,O1)	1.364	1.359	−0.4	1.350	−1.0	1.351	−0.6	1.343	−0.5
R(C4,H)	1.100	1.088	−1.1	1.087	−1.2	1.087	0.0	1.086	0.0
A(C4,C1,O3)	126.6	126.2	−0.3	126.2	−0.4	125.9	−0.2	125.9	−0.2
A(C4,C1,O1)	110.6	111.5	0.8	111.7	1.0	111.9	0.4	112.1	0.4
(d) Ethanol (Expr. from [45])									
R(C2,C3)	1.512	1.517	0.3	1.511	−0.1	1.517	0.0	1.511	0.0
R(C3,H)	1.090	1.093	0.2	1.091	0.1	1.093	0.0	1.092	0.1
R(C2,H)	1.100	1.099	−0.1	1.097	−0.3	1.097	−0.2	1.095	−0.2
R(C2,O2)	1.431	1.431	0.0	1.422	−0.6	1.438	0.5	1.430	0.5
R(O2,H1)	0.971	0.962	−1.0	0.960	−1.2	0.963	0.2	0.962	0.2
A(C2,C3,H)	110.0	110.5	0.5	110.4	0.4	110.8	0.3	110.7	0.3
A(C3,C2,H)	111.0	110.1	−0.8	110.2	−0.8	110.4	0.2	110.4	0.2
A(C3,C2,O2)	107.8	108.0	0.2	107.9	0.1	108.4	−0.4	108.3	0.4

Table 4
The charge population (in unit e) at selected atoms in ground state from NBO calculations.

Atom	DFT			DFT + PCM			
	XC1g	XC2g	Δ_{21}	XC1s	Δ_{sg}	XC2b	Δ_{sg}
(a) Ethyl acetate, Et2(1-abc)							
O1	−0.600	−0.609	−0.009	−0.650	−0.050	−0.659	−0.009
O2	−0.575	−0.580	−0.005	−0.571	0.004	−0.576	−0.005
C1	0.809	0.822	0.013	0.826	0.017	0.840	0.014
C2	−0.034	−0.039	−0.005	−0.034	0.000	−0.039	−0.005
C3	−0.590	−0.598	−0.008	−0.593	−0.003	−0.602	−0.009
C4	−0.668	−0.677	−0.009	−0.672	−0.004	−0.682	−0.010
(b) Water							
H1	0.457	0.460	0.003	0.477	0.020	0.480	0.020
O3	−0.913	−0.920	−0.007	−0.953	−0.040	−0.960	−0.040
(c) Acetic acid, Ca2(1)							
O1	−0.696	−0.703	−0.007	−0.697	−0.001	−0.704	−0.001
O3	−0.595	−0.604	−0.009	−0.643	−0.048	−0.652	−0.048
C1	0.799	0.811	0.012	0.817	0.018	0.830	0.019
C4	−0.679	−0.688	−0.009	−0.682	−0.003	−0.693	−0.005
(d) Ethanol							
H1	0.455	0.459	0.004	0.473	0.018	0.477	0.018
O2	−0.743	−0.748	−0.005	−0.776	−0.033	−0.781	−0.033
C2	−0.023	−0.027	−0.004	−0.024	−0.001	−0.029	−0.002
C3	−0.592	−0.600	−0.008	−0.596	−0.004	−0.605	−0.005

While our results show the dominance of the long-range interaction in the individual molecule, the increasing E compensates each other, hence the net energy of the product and the reactant (reaction energy) is relatively constant. The reaction energy is +0.08 eV and +0.10 eV from XC1g and XC2g calculations, respectively. The long-range correction insignificantly raises the value by 0.02 eV.

The effect of surrounding water. We also provide the results of DFT coupled with PCM in Table 3 (geometry), Table 4 (charge population), and Fig. 5 (level energy diagram). The geometry does not change (most values of err. are less than 0.5%) with respect to the calculation in the gas phase. The number of charge changes at some atoms by an order of 10^{-2} e and this is significantly changes the frontier molecular orbital wave functions as we have encountered in our previous studies [37, 38]. The perturbation from surrounding waters stabilizes the individual molecule in such a way that the net energy does not change. The reaction energy is 0.10 eV and 0.12 eV with XC1s and XC2s, respectively. The long-range correction improves the value by 0.02 eV, which is exactly the same value in the gas phase case.

Table 5
Charge population from NBO calculation at C1 and C4 of the conformers in the ground state.

Conformer	C1			C4		
	XC1g	XC2g	Δ_{21}	XC1g	XC2g	Δ_{21}
Et1(1)	0.664	0.673	0.009	0.116	0.120	0.004
Et1(2)	0.661	0.670	0.009	0.117	0.122	0.005
Et2(1-a)	0.809	0.822	0.013	−0.668	−0.677	−0.009
Et2(2-a)	0.808	0.821	0.013	−0.668	−0.677	−0.009
Et3(1-a)	0.769	0.805	0.036	−0.447	−0.458	−0.011
Et3(1-b)	0.770	0.801	0.031	−0.421	−0.436	−0.015
Et3(1-c)	0.770	0.801	0.031	−0.421	−0.436	−0.015
Et3(2-a)	0.768	0.804	0.036	−0.447	−0.459	−0.012
Et3(2-b)	0.769	0.801	0.032	−0.422	−0.437	−0.015
Et3(2-c)	0.769	0.800	0.031	−0.421	−0.435	−0.014
Et4(1-a)	0.792	0.781	−0.011	0.006	0.002	−0.004
Et4(1-b)	0.786	0.783	−0.003	0.006	0.002	−0.004
Et4(1-c)	0.786	0.783	−0.003	0.006	0.002	−0.004
Et4(2-a)	0.791	0.781	−0.010	0.006	0.001	−0.005
Et4(2-b)	0.786	0.782	−0.004	0.006	0.002	−0.004
Et4(2-c)	0.785	0.782	−0.003	0.006	0.002	−0.004

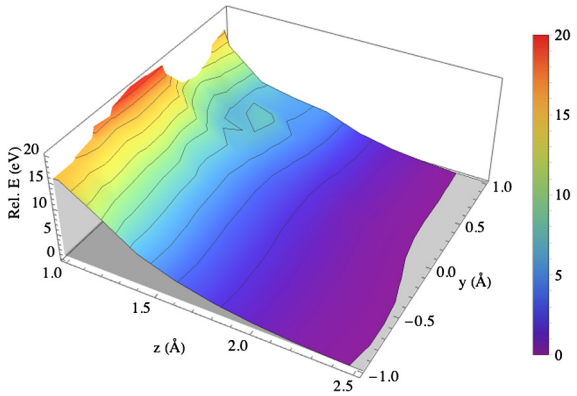

Fig. 4. Potential energy surface of water molecule attacking the electrophilic site of ethyl acetate according to Fig. 1a scenario.

3.2. On the transition state structure

The typical optimized geometry of [Et–W] complex at the saddle point is presented in Fig. 1b. All results have one imaginary frequency as it is required for a TS structure. All imaginary frequencies belong to the normal mode involving the motion of H1 between O2 and O3. The geometry provides us some possible conformers of the [Et–W] complex. Our calculations determine more than one optimized conformer of each [Et–W] complex: two for [Et1–W] and [Et2–W] and three for [Et3–W] and [Et4–W]. Optimization calculations always end up with water in the positive z-axis in the gauche conformation and orientate CH_3 at C4 to either the (a) staggered or (d) eclipsed conformation.

The IRC calculations ensure the optimized geometries of [Et–W] are at the correct transition state according to Scheme 1. Fig. 6 shows the IRC calculation results (only two extreme cases plotted for [Et3–W] and [Et4–W]). All transition state geometries lead exactly to state **1a** and **1c**. Therefore, Fig. 1b is indeed the typical geometry at state **1b**.

Table 6, 7, 8, and 9 display four important geometrical parameters of [Et–W] in the transition state. They are the distance of C1–O2 (R_1), O3–H1 (R_2), C1–O3 (R_3), and O2–H1 (R_4), respectively. The favorable condition for hydrolysis is the elongation of R_1 and R_2 with respect to the state **1a** and a short distance of R_3 and R_4. In case of Et2, using XC1g, R_1 and R_2 significantly elongate to 33.2% and 27.8%, respectively. R_1 and R_2 in all [Et–W] complexes are 1.73 Å and 1.19 Å on average, respectively. Since C⋯O in gas phase experimentally 1.48 Å [45], all [Et–W] complexes show a tendency to cleavage Et forming Ca and ethanol. Meanwhile, R_3 and R_4 determine the stability of transition state geometry: the shorter the values, the stronger the interaction between Et and W in [Et–W] complexes, which implies more stable geometry. In that sense, the most stable conformation is gauche (in case of [Et1–W] and [Et2–W]) and eclipsed with a halogen atom at "e" position (in case of [Et3–W] and [Et2–W]).

The effect of long-range correction and surrounding water. The value of $err._{21}$ and $err._{sg}$ in Table 6, 7, 8, and 9 show the effect of the long-range correction and the surrounding water. Overall, the effect is more significant in [Et–W] complex (state **1b**) than in individual molecules of Et and W (state **1a**) and Ca and alcohol (state **1c**). The significant effect of the long-range correction is on R_1 and R_3. Both parameters involve C⋯O bond. When we consider the ground state analysis (Fig. 5), the results show a tendency of XC1s significantly affecting molecules with C⋯O bond. It explains qualitatively as to how XC1s raises E of ethyl acetate almost twice as much as the acetic acid and ethanol (see Fig. 5): ethyl acetate has two C⋯O bonds, acetic acid has one O⋯C⋯O, and ethanol only has one C⋯O.

We extend the discussion on [Et2–W] geometry in the transition state. Our results are comparable with the work of Yamabe et al. [14]. Table 10 resumes the comparison between these two works. Overall, our results are far from the results of [14]. In the water surrounding model, it is clear that PCM and Onsager's model yields a significant difference in geometry. The difference can be understood as follows. Both PCM and Onsager's model create a cavity to simulate the reaction field, but the method to make the cavity is completely different.

3.3. On the conformational effect

We evaluate the conformational effect on geometry based on the value of range in Table 6, 7, 8, and 9. The wider the range means the more significant the conformer variation of the complex. In our case, the overall range is in an order of 10^{-2} Å. Furthermore, we find two trends. First, the range is wider in the presence of a halogen atom (Et3 and Et4). Second, the long-range correction and the surrounding water significantly affect the ranges of R_1 and R_2 of [Et1–W] and [Et2–W]. These two trends imply that the conformer of ethyl acetate has a significant effect when it is forming a complex with water in the transition state. Accordingly, the figure 10^{-2} Å is a significant range for this study.

The difference in geometry directly affects the activation energy ($\Delta^{\ddagger}G°$) as displayed in Table 11. We highlight three points from the table as follows.

First of all, there is a general trend of $\Delta^{\ddagger}G°$ in the presence of the halogen atom in esters. This result is consistent with the charge population at C1 of ester in the ground state (Table 5) and R_3 (Table 6). Charge population at C1 is more negative in the presence of halogen atom (Et2 versus Et3 and Et4), so it provides more charges to form a

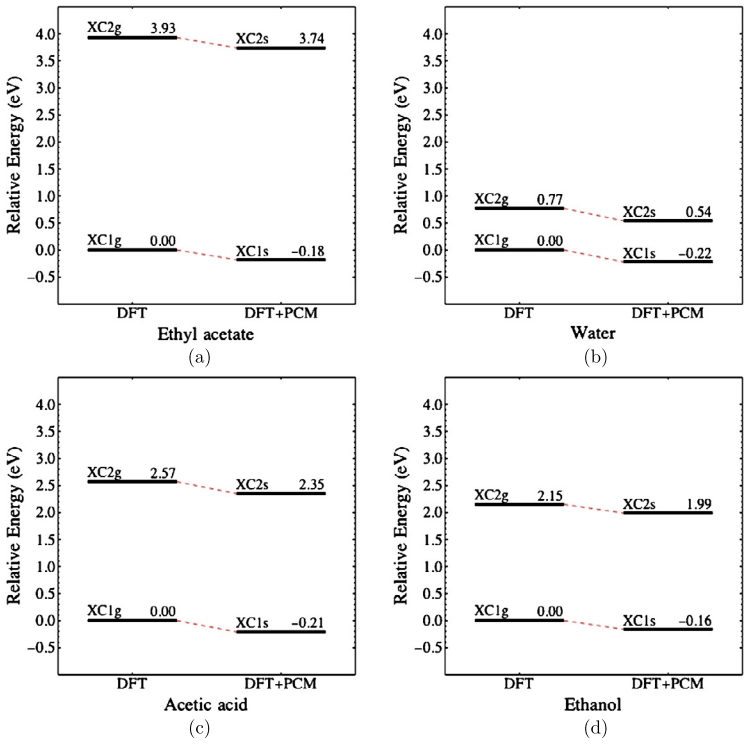

Fig. 5. Energy level diagram of molecules in Table 3, for (a) ethyl acetate, (b) water, (c) acetic acid, and (d) ethanol. The calculated energy by XC1g is set to be the reference.

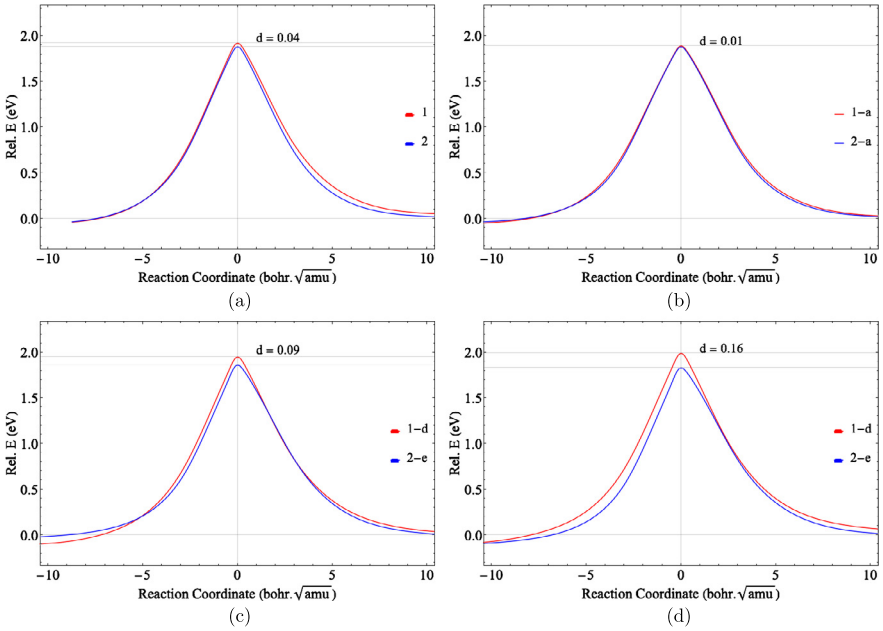

Fig. 6. Reaction path calculations based on the optimized geometry of [Et–W] complexes for the case of (a) Et1, (b) Et2, (c) Et3, and (d) Et4 with the conformations are shown in the legend. The peak of path is the saddle point which is the transition state (**1b**), to the left is the initial state (**1a**) and to the right is the final state (**1c**). The energy reference is the **1a** of each system, so the height corresponds to the energy barrier of each reaction with d as the difference in energy barrier between two different conformers. (Table 11 lists the complete value of energy barrier for all reactions of interest.)

covalent bond with O3 from H_2O (shorter R_3). The elongation of R_1 (Table 6) supports the C1–O3 bonding formation and directly determines the value of $\Delta^{\ddagger}G°$. There is an exception in "d" conformation, where R_1 is shorter, making the $\Delta^{\ddagger}G°$ higher than the other conformations. However, the overall trend is the presence of a halogen atom lowers $\Delta^{\ddagger}G°$, which corresponds to the higher $k(T)$. This is in line with other esters [4, 5, 6] as mentioned in the introduction. Furthermore, a heavier halogen atom raises $k(T)$ which agrees with the result by Schmeer and Sturm [12]. This part of results is important in our study because it justifies our calculation method.

Secondly, a comparison among results in the table shows the effect of the long-range correction and the surrounding water. The former's effect alone ($err._{21}$) is less than 1% on average, while the latter's effect ($err._{sg}$) is more than 7% on average. Even though $err._{21}$ in this work is insignificant, the exchange-correlation functional is still an important factor. As we see in Schmeer and Sturm [12], the use of Hatree-

Table 6
Distance of C1–O2 in the transition state (R_1, in Å).

Conformer	DFT			DFT + PCM			
	XC1g	XC2g	err.$_{21}$	XC1s	err.$_{sg}$	XC2b	err.$_{sg}$
(1) [Et1–W]							
(1)	1.715	1.663	−3.0	1.664	−3.0	1.615	−2.9
(2)	1.720	1.668	−3.0	1.677	−2.5	1.626	−2.5
range	0.004	0.005		0.013		0.012	
(2) [Et2–W]							
(1-a)	1.791	1.727	−3.6	1.746	−2.5	1.668	−3.4
(2-d)	1.793	1.726	−3.7	1.759	−1.9	1.680	−2.7
range	0.001	0.001		0.012		0.012	
(3) [Et3–W]							
(1-f)	1.764	1.703	−3.5	1.677	−4.9	1.619	−5.0
(1-d)	1.695	1.640	−3.2	1.654	−2.4	1.602	−2.3
(1-e)	1.712	1.654	−3.4	1.659	−3.1	1.607	−2.8
(2-f)	1.764	1.701	−3.6	1.690	−4.2	1.630	−4.1
(2-d)	1.699	1.644	−3.2	1.665	−2.0	1.612	−2.0
(2-e)	1.713	1.654	−3.4	1.671	−2.5	1.617	−2.3
range	0.069	0.063		0.035		0.028	
(4) [Et4–W]							
(1-f)	1.771	1.706	−3.7	1.692	−4.5	1.627	−4.6
(1-d)	1.687	1.636	−3.0	1.642	−2.6	1.595	−2.5
(1-e)	1.712	1.654	−3.4	1.657	−3.2	1.607	−2.8
(2-f)	1.771	1.704	−3.8	1.705	−3.7	1.639	−3.8
(2-d)	1.690	1.637	−3.1	1.653	−2.2	1.604	−2.0
(2-e)	1.717	1.659	−3.4	1.673	−2.6	1.619	−2.4
range	0.084	0.070		0.062		0.044	

Table 7
Distance of O3–H1 in the transition state (R_2, in Å).

Conformer	DFT			DFT + PCM			
	XC1g	XC2g	err.$_{21}$	XC1s	err.$_{sg}$	XC2b	err.$_{sg}$
(1) [Et1–W]							
(1)	1.236	1.232	−0.3	1.263	2.2	1.245	1.1
(2)	1.227	1.221	−0.4	1.248	1.8	1.231	0.7
range	0.009	0.010		0.015		0.014	
(2) [Et2–W]							
(1-a)	1.228	1.224	−0.4	1.268	3.2	1.257	2.6
(2-d)	1.225	1.223	−0.2	1.258	2.7	1.245	1.8
range	0.004	0.001		0.011		0.011	
(3) [Et3–W]							
(1-f)	1.210	1.203	−0.6	1.251	3.4	1.237	2.8
(1-d)	1.234	1.229	−0.4	1.252	1.5	1.235	0.5
(1-e)	1.261	1.256	−0.4	1.267	0.5	1.247	−0.7
(2-f)	1.208	1.205	−0.3	1.238	2.5	1.226	1.7
(2-d)	1.227	1.221	−0.5	1.241	1.2	1.225	0.4
(2-e)	1.256	1.250	−0.5	1.256	0.0	1.236	−1.1
range	0.053	0.052		0.029		0.021	
(3) [Et4–W]							
(1-f)	1.203	1.200	−0.2	1.238	2.9	1.231	2.6
(1-d)	1.231	1.223	−0.6	1.248	1.4	1.231	0.6
(1-e)	1.268	1.258	−0.8	1.280	1.0	1.252	−0.5
(2-f)	1.201	1.201	0.0	1.226	2.1	1.219	1.5
(2-d)	1.227	1.221	−0.5	1.239	1.0	1.224	0.2
(2-e)	1.261	1.252	−0.7	1.267	0.5	1.243	−0.7
range	0.066	0.058		0.054		0.033	

Fock method resulted in 58.74 kcal/mol and 64.47 kcal/mol of $\Delta^{\ddagger}G°$.[1] Furthermore, the method to model the water surrounding is also important. The use of Onsager's model by Yamabe et al. [14] resulted in 47.90 kcal/mol. The difference in $\Delta^{\ddagger}G°$ is expected since the geometry is also different (see Table 10).

Lastly, the range of $\Delta^{\ddagger}G°$ displays the effect of conformation. In XC1g, the range is 0.72, 1.07, 2.64, and 3.47 kcal/mol for Et1, Et2, Et3, and Et4 case, respectively. These figures give a significant ratio between the highest and the lowest $k(T)$ of each case. Since $k(T)$ is an exponential function of negative $\Delta^{\ddagger}G°$ [see Equation (1)], 0.72 kcal/mol (in gas phase) corresponds to 3 times increment of the rate con-

[1] Schmeer and Sturm [12] used two waters and has one intermediate state and two transition states in the reaction path. The calculations were in the gas phase.

Table 8
Distance of C1–O3 in the transition state (R_3, in Å).

Conformer	DFT			DFT + PCM			
	XC1g	XC2g	$err._{21}$	XC1s	$err._{sg}$	XC2b	$err._{sg}$
(1) [Et1–W]							
(1)	1.780	1.731	−2.8	1.779	−0.1	1.711	−1.2
(2)	1.773	1.724	−2.8	1.771	−0.1	1.702	−1.3
range	0.007	0.008		0.008		0.009	
(2) [Et2–W]							
(1-a)	1.841	1.780	−3.3	1.859	1.0	1.776	−0.3
(2-d)	1.838	1.780	−3.2	1.859	1.1	1.775	−0.3
range	0.002	0.001		0.001		0.001	
(3) [Et3–W]							
(1-f)	1.775	1.714	−3.4	1.763	−0.7	1.692	−1.3
(1-d)	1.760	1.707	−3.0	1.756	−0.2	1.686	−1.2
(1-e)	1.829	1.771	−3.2	1.792	−2.0	1.717	−3.1
(2-f)	1.774	1.717	−3.2	1.757	−1.0	1.686	−1.8
(2-d)	1.755	1.701	−3.1	1.752	−0.2	1.681	−1.2
(2-e)	1.824	1.766	−3.2	1.789	−1.9	1.712	−3.1
range	0.074	0.070		0.040		0.035	
(4) [Et4–W]							
(1-f)	1.775	1.716	−3.3	1.759	−0.9	1.690	−1.5
(1-d)	1.749	1.695	−3.1	1.739	−0.5	1.671	−1.4
(1-e)	1.835	1.772	−3.4	1.808	−1.5	1.724	−2.7
(2-f)	1.774	1.718	−3.2	1.754	−1.2	1.687	−1.8
(2-d)	1.746	1.694	−3.0	1.736	−0.6	1.670	−1.4
(2-e)	1.832	1.773	−3.3	1.806	−1.4	1.726	−2.6
range	0.088	0.079		0.072		0.055	

Table 9
Distance of O2–H1 in the transition state (R_4, in Å).

Conformer	DFT			DFT + PCM			
	XC1g	XC2g	Δ_{21}	XC1s	Δ_{sg}	XC2b	Δ_{sg}
(1) [Et1–W]							
(1)	1.187	1.185	−0.2	1.169	−1.6	1.181	−0.3
(2)	1.195	1.194	−0.1	1.180	−1.2	1.192	−0.1
range	0.008	0.009		0.011		0.012	
(2) [Et2–W]							
(1-a)	1.190	1.187	−0.3	1.158	−2.7	1.163	−2.0
(2-d)	1.192	1.187	−0.4	1.165	−2.3	1.171	−1.3
range	0.002	0.000		0.007		0.008	
(3) [Et3–W]							
(1-f)	1.212	1.213	0.1	1.181	−2.5	1.191	−1.8
(1-d)	1.193	1.192	−0.1	1.180	−1.1	1.193	0.0
(1-e)	1.167	1.166	−0.1	1.167	0.1	1.182	1.4
(2-f)	1.213	1.210	−0.2	1.175	−3.1	1.200	−0.9
(2-d)	1.199	1.199	0.0	1.199	0.0	1.200	0.1
(2-e)	1.170	1.170	−0.0	1.170	−0.0	1.190	1.7
range	0.046	0.048		0.032		0.018	
(4) [Et4–W]							
(1-f)	1.218	1.215	−0.2	1.191	−2.2	1.195	−1.7
(1-d)	1.197	1.199	0.2	1.186	−0.9	1.199	−0.0
(1-e)	1.160	1.163	0.2	1.156	−0.4	1.176	1.1
(2-f)	1.218	1.213	−0.5	1.200	−1.5	1.204	−0.7
(2-d)	1.200	1.201	0.1	1.193	−0.6	1.204	0.3
(2-e)	1.164	1.166	0.1	1.164	0.0	1.181	1.3
range	0.058	0.053		0.044		0.028	

Table 10
Result comparison on [Et2–W] in the transition state.

Parameter	Ref. [14]	XC1s	err.	XC2s	err.
R_1	1.790	1.746	−2.4	1.668	−6.8
R_2	1.203	1.268	5.4	1.257	4.4
R_3	1.802	1.859	3.2	1.776	−1.5
R_4	1.221	1.158	−5.2	1.163	−4.7

Here err. is the error percentage with respect to the value from Ref. [14].

Table 11
The standard Gibbs activation energy (in kcal/mol) from various [Et–W] conformers.

Conformer	DFT			DFT + PCM			
	XC1g	XC2g	$err._{21}$	XC1s	$err._{1sg}$	XC2b	$err._{2sg}$
(1) Et1 + W → [Et1–W] → Ca1 + ethanol							
(1)	52.93	53.29	0.7	56.77	7.3	56.78	6.5
(2)	52.21	52.44	0.4	55.67	6.6	55.81	6.4
range	0.72	0.85		1.10		0.96	
(2) Et2 + W → [Et2–W] → Ca2 + ethanol							
(1-a)	53.52	54.01	0.9	57.64	7.7	57.92	7.2
(2-d)	52.45	53.05	1.1	56.18	7.1	56.95	7.3
range	1.07	0.97		1.46		0.97	
(3) Et3 + W → [Et3–W] → Ca3 + ethanol							
(1-f)	53.42	53.89	0.9	57.93	8.4	57.72	7.1
(1-d)	54.86	54.35	−0.9	58.47	6.6	57.72	6.2
(1-e)	53.46	53.37	−0.2	57.80	8.1	57.13	7.0
(2-f)	52.80	53.02	0.4	56.90	7.8	56.87	7.3
(2-d)	53.67	53.53	−0.3	56.95	6.1	56.52	5.6
(2-e)	52.22	52.44	0.4	57.79	10.7	56.35	7.5
range	2.64	1.91		1.58		1.37	
(4) Et4 + W → [Et4–W] → Ca4 + ethanol							
(1-f)	53.10	53.57	0.9	57.57	8.4	57.28	6.9
(1-d)	55.28	54.91	−0.7	59.48	7.6	58.42	6.4
(1-e)	52.76	52.93	0.3	56.42	6.9	56.69	7.1
(2-f)	52.48	52.57	0.2	56.62	7.9	56.13	6.8
(2-d)	54.83	54.43	−0.7	58.12	6.0	57.43	5.5
(2-e)	51.81	51.96	0.3	55.83	7.8	56.19	8.1
range	3.47	2.96		3.66		2.29	

Table 12
The rate constant at 298.15 K in natural logarithmic value.

Conformer	DFT			DFT + PCM			
	XC1g	XC2g	$rat._{21}$	XC1s	$rat._{1sg}$	XC2b	$rat._{2sg}$
(1) Et1 + W → [Et1–W] → Ca1 + ethanol							
(1)	−59.88	−60.49	−0.61	−66.36	−6.48	−66.38	−5.89
(2)	−58.66	−59.05	−0.39	−64.50	−5.84	−64.74	−5.69
$rat._k$	3.37	4.20		6.40		5.14	
(2) Et2 + W → [Et2–W] → Ca2 + ethanol							
(1-a)	−60.87	−61.70	−0.83	−67.83	−6.95	−68.30	−6.60
(2-d)	−59.07	−60.08	−1.01	−65.36	−6.30	−66.66	−6.58
$rat._k$	6.09	5.05		11.75		5.14	
(3) Et3 + W → [Et3–W] → Ca3 + ethanol							
(1-f)	−60.71	−61.50	−0.79	−68.32	−7.61	−67.96	−6.46
(1-d)	−63.14	−62.27	0.86	−69.23	−6.09	−67.96	−5.69
(1-e)	−60.77	−60.62	0.15	−68.10	−7.33	−66.97	−6.35
(2-f)	−59.66	−60.03	−0.37	−66.58	−6.92	−66.53	−6.50
(2-d)	−61.13	−60.89	0.24	−66.66	−5.54	−65.94	−5.05
(2-e)	−58.68	−59.05	−0.37	−68.08	−9.40	−65.65	−6.60
$rat._k$	86.13	25.12		14.15		10.09	
(3) Et4 + W → [Et4–W] → Ca4 + ethanol							
(1-f)	−60.17	−60.96	−0.79	−67.71	−7.54	−67.22	−6.26
(1-d)	−63.84	−63.22	0.62	−70.93	−7.09	−69.14	−5.92
(1-e)	−59.59	−59.88	−0.29	−65.77	−6.18	−66.22	−6.35
(2-f)	−59.12	−59.27	−0.15	−66.11	−6.99	−65.28	−6.01
(2-d)	−63.08	−62.41	0.68	−68.64	−5.55	−67.47	−5.06
(2-e)	−57.99	−58.24	−0.25	−64.77	−6.79	−65.38	−7.14
$rat._k$	349.57	145.33		473.66		47.71	

stant (at 298.15 K), 1.07 kcal/mol corresponds to 6 times increment, 2.64 kcal/mol corresponds to 86 times increment, and 3.47 kcal/mol corresponds to 350 times increment. Table 12 tabulates these results and clarifies the effect of conformation. Overall, the long-range correction and the surrounding water narrow the range, but the figures are still significant. Meanwhile, the gauche conformation has the highest $k(T)$ and the halogen atom prefers in "e" position (staggered conformation, see Fig. 3).

4. Conclusion

We have reported the conformation in transition state significantly affects the activation energy of ethyl acetate neutral hydrolysis. The gauche conformers tend to have higher rate constant than the trans ones. This leads to the significant ratio between the lowest and the highest rate constant: from 3 to 350 times, or from 4 to 145 times after long-range correction (all in the gas phase). We argued that one must

take the conformers into the consideration to study the ester neutral hydrolysis. Furthermore, the halogenated ethyl acetate has higher rate constant and the halogen atom prefers in the staggered conformation. The halogenation effect from our calculations is in agreement with experimental data for other ester variant. Finally, we also presented the long-range interaction and PCM to model the surrounding water stabilize the transition state geometry but raise the activation energy from 5.5% to 8.1%.

Declarations

Author contribution statement

Febdian Rusydi: Conceived and designed the experiments; Performed the experiments; Analyzed and interpreted the data; Contributed reagents, materials, analysis tools or data; Wrote the paper.

Nufida Dwi Aisyah, Rizka Fadilla: Conceived and designed the experiments; Performed the experiments.

Hermawan Dipojono, Mudasir Mudasir, Andrivo Rusydi: Analyzed and interpreted the data.

Faozan Ahmad, Ira Puspitasari: Contributed reagents, materials, analysis tools or data.

Funding statement

This work was supported by Directorate General of Higher Education, Research, and Technology Ministry, Republic of Indonesia through National Collaboration Research Grant number 563/UN3.14/LT/2018.

Competing interest statement

The authors declare no conflict of interest.

Additional information

No additional information is available for this paper.

Acknowledgements

Authors thank to Lusia Silfia Pulo Boli (Research Center for Quantum Engineering Design, Universitas Airlangga, Surabaya, Indonesia), Vera Khoirunisa (Engineering Physics Department, Institut Teknologi Sumatera, Lampung, Indonesia), Dr. Adhitiya Gandaryus Saputro and Dr. Muhammad Kemal Agusta (Engineering Physics Department, Institut Teknologi Bandung, Bandung, Indonesia), Prof. Azizan Ahmad (Chemistry Department, Universiti Kebangsaan Malaysia, Malaysia), and Prof. Diño Wilson Agerico Tan and Prof. Yoshitada Morikawa (Precission Science & Technology and Applied Physics, Graduate School of Engineering, Osaka University, Japan) for their insight and valuable discussions. RNF particularly thanks to LPDP for the scholarship. All calculations using Gaussian 09 software are performed in the computer facility at the Osaka University.

References

[1] Y.H. Hsieh, N. Weinberg, S. Wolfe, The neutral hydrolysis of methyl acetate – Part 1. Kinetic experiments, Can. J. Chem. 87 (2009) 539–543.
[2] A. Skrabal, A. Zahorka, Die Wasserverseifung des Athylazetats, Monatsh. Chem. 53–54 (1929).
[3] R. Wolfenden, Y. Yuan, The “neutral” hydrolysis of simple carboxylic esters in water and the rate enhancements produced by acetylcholinesterase and other carboxylic acid esterases, J. Am. Chem. Soc. 133 (2011) 13821–13823.
[4] A. Moffat, H. Hunt, Solvent and chain length effects in the non-catalyzed hydrolysis of some alkyl and aryl trifluoroacetates, J. Am. Chem. Soc. 81 (1959) 2082–2086.
[5] E.K. Euranto, N.J. Cleve, Kinetics of the neutral hydrolysis of chloromethyl chloroacetate, Acta Chem. Scand. 17 (1963) 1584–1594.
[6] K.S. Venkatasubban, K.R. Davis, J.L. Hogg, Transition-state structure for the neutral water-catalyzed hydrolysis of ethyl trifluorothiolacetate, J. Am. Chem. Soc. 100 (1963) 6125–6128.
[7] J.F. Kirsch, W.P. Jencks, Nonlinear structure-reactivity correlations. The imidazole-catalyzed hydrolysis of esters, J. Am. Chem. Soc. 86 (1964).
[8] P.L. da Silva, L. Guimarães, J.R.P. Jr., Revisiting the mechanism of neutral hydrolysis of esters: water autoionization mechanisms with acid or base initiation pathways, J. Phys. Chem. B 117 (2013) 6487–6497.
[9] Z. Shi, Y.H. Hsieh, N. Weinberg, S. Wolfe, The neutral hydrolysis of methyl acetate - Part 2. Is there a tetrahedral intermediate? Can. J. Chem. 87 (2009) 544–555.
[10] Y.-H. Hsieh, N. Weinberg, K. Yang, C.-K. Kim, Z. Shi, S. Wolfe, Hydration of the carbonyl group – acetic acid catalysis in the co-operative mechanism, Can. J. Chem. 83 (2005) 769–785.
[11] X. Chen, C.-G. Zhan, Fundamental reaction pathways and free-energy barriers for ester hydrolysis of intracellular second-messenger 3–5–cyclic nucleotide, J. Phys. Chem. A 108 (2004) 3789–3797.
[12] G. Schmeer, P. Sturm, A quantum chemical approach to the water assisted neutral hydrolysis of ethyl acetate and its derivatives, Phys. Chem. Chem. Phys. 1 (1999) 1025–1030.
[13] S. Wolfe, C.-K. Kim, K. Yang, N. Weinberg, Z. Shi, Hydration of the carbonyl group. A theoretical study of the cooperative mechanism, J. Am. Chem. Soc. 115 (1995) 4240–4260.
[14] S. Yamabe, N. Tsuchida, Y. Hayashida, Reaction paths of the water-assisted neutral hydrolysis of ethyl acetate, J. Phys. Chem. A 109 (2005) 7216–7224.
[15] C.-G. Zhan, D.W. Landry, R.L. Ornstein, Energy barriers for alkaline hydrolysis of carboxylic acid esters in aqueous solution by reaction field calculations, J. Phys. Chem. A 104 (2000) 7672–7678.
[16] B. Kallies, R. Mitzner, Models of water-assisted hydrolyses of methyl formate, formamide, and urea from combined DFT-SCRF calculations, J. Mol. Model. 4 (1998).
[17] R.T. Bartus, R.L. Dean, B. Beer, A.S. Lippa, The cholinergic hypothesis of geruatric memory dysfunction, Science 217 (1982) 408–417.
[18] P.T. Francis, A.M. Palmer, M. Snape, G.K. Wilcock, The cholinergic hypothesis of Alzheimer – disease: a review of progress, J. Neurol. Neurosurg. Psychiatry 66 (1999) 137–147.
[19] T. Svinning, H. Sorum, A reinvestigation of the crystal structure of acetylcholine bromide, Acta Crystallogr., Sect. B 31 (1975) 1581–1585.
[20] M. Sax, M. Rodrigues, G. Blank, M.K. Wood, J. Pletcher, The conformation of acetylcholine and the crystal structure of 2, 2-dimethylbutyl 3, 5-dinitrobenzoate, Acta Crystallogr., Sect. B 32 (1976) 1953–1956.
[21] R.W. Behling, T. Yamane, G. Navon, L.W. Jelinski, Conformation of acetylcholine bound to the nicotinic acetylcholine receptor, Proc. Natl. Acad. Sci. 85 (1988) 6721–6725.
[22] K.J. Wilson, P. Derreumaux, G. Vergoten, W.L. Peticolas, Conformational studies of neuroactive ligands 2. solution-state conformations of acetylcholine, J. Phys. Chem. 93 (1989) 1351–1357.
[23] B. Hernández, P. Houzé, F. Pflëger, S.G. Kruglik, M. Ghomi, Raman scattering-based multiconformational analysis for probing the structural differences between acetylcholine and acetylthiocholine, J. Pharm. Biomed. Anal. 138 (2017) 54–62.
[24] H. Sorum, The crystal and molecular structure of acetyl choline bromide, Acta Chem. Scand. 13 (1959) 345–359.
[25] C. Chothia, P. Pauling, Conformation of cholinergic molecules relevant to acetylcholinesterase, Nature 223 (1969) 919–921.
[26] C. Chothia, P. Pauling, The conformation of cholinergic molecules at nicotinic nerve receptors, Proc. Nat. Acad. Sci. 65 (1970) 477–482.
[27] T.L. Lemke, D.A. William, V.F. Roche, S.W. Zito (Eds.), Foye’s Principle of Medicinal Chemistry, 7th ed., Lippincott Williams & Wilkins, 2013.
[28] P. Hohenberg, W. Kohn, Inhomogeneous electron gas, Phys. Rev. 136 (1964) B864.
[29] W. Kohn, L.J. Sham, Self-consistent equations including exchange and correlation effects, Phys. Rev. A 140 (1965) A1133.
[30] M.J. Frisch, G.W. Trucks, H.B. Schlegel, G.E. Scuseria, J.R.C.M.A. Robb, G. Scalmani, V. Barone, B. Mennucci, G.A. Petersson, H. Nakatsuji, M. Caricato, X. Li, H.P. Hratchian, A.F. Izmaylov, J. Bloino, G. Zheng, J.L. Sonnenberg, M. Hada, M. Ehara, K. Toyota, R. Fukuda, J. Hasegawa, M. Ishida, T. Nakajima, Y. Honda, O. Kitao, H. Nakai, T. Vreven, J.A. Montgomery Jr., J.E. Peralta, F. Ogliaro, M. Bearpark, J.J. Heyd, E. Brothers, K.N. Kudin, V.N. Staroverov, T. Keith, R. Kobayashi, J. Normand, K. Raghavachari, A. Rendell, J.C. Burant, S.S. Iyengar, J. Tomasi, M. Cossi, N. Rega, J.M. Millam, M. Klene, J.E. Knox, J.B. Cross, V. Bakken, C. Adamo, J. Jaramillo, R. Gomperts, R.E. Stratmann, O. Yazyev, A.J. Austin, R. Cammi, C. Pomelli, J.W. Ochterski, R.L. Martin, K. Morokuma, V.G. Zakrzewski, G.A. Voth, P. Salvador, J.J. Dannenberg, S. Dapprich, A.D. Daniels, O. Farkas, J.B. Foresman, J.V. Ortiz, J. Cioslowski, D.J. Fox, Gaussian 09, revision c. 01, 2010, “Gaussian Inc. Wallingford CT”.
[31] A.D. Becke, Density–functional thermochemistry. iii. The role of exact exchange, J. Chem. Phys. 98 (1993) 5648–5652.
[32] T. Yanaia, D.P. Tew, N.C. Handy, A new hybrid exchange–correlation functional using the coulomb-attenuating method (cam-b3lyp), Chem. Phys. Lett. 393 (2004) 51–57.
[33] A.G. Saputro, F. Rusydi, M.K. Agusta, H. Kasai, H.K. Dipojono, Oxygen reduction reaction on cobalt-(6) pyrrol cluster: density functional theory study, J. Phys. Soc. Jpn. 81 (2012) 034703.
[34] F. Rusydi, M.K. Agusta, A.G. Saputro, H. Kasai, A first principle study on zinc porphyrin interaction with O_2 in zinc porphyrin(oxygen) complex, J. Phys. Soc. Jpn. 81 (2012) 124301.

[35] F. Rusydi, M.K. Agusta, A.G. Saputro, H. Kasai, A theoretical study of ligand effects on the electronic structures of ligated zinc porphyrin using density functional theory, J. Vac.Soc. Jpn. 57 (2014) 102–110.
[36] W.-F. Mark-Lee, F. Rusydi, L.J. Minggu, T. Kubo, M. Kassim, Bis(bipyridyl)-ru(ii)-benzoyl-3-(pyridine-2-yl)-1h-pyrazile as potential photosensitiser: experimental and density functional theory study, J. Technol. 75 (2017) 117–123.
[37] F. Rusydi, A.G. Saputro, H. Kasai, A density-functional study on the change of q/b-band intensity ratio of zinc tetraphenylporphyrin in solvents, J. Phys. Soc. Jpn. 83 (2014) 084802.
[38] F. Rusydi, G. Shukri, A.G. Saputro, H.K. Dipojono, S. Suprijadi, Dipole strength calculation based on two-level system approximation to study q/b-band intensity ratio of zntbp in solvent, J. Phys. Soc. Jpn. 86 (2017) 044706.
[39] R.N. Fadilla, N.D. Aisyah, H.K. Dipojono, F. Rusydi, A theoretical study of the rearranging trans-HCOH to H_2CO via quantum tunneling with dft and wkb approximation, Proc. Eng. 170 (2017) 113–118.
[40] N.D. Aisyah, R.N. Fadilla, H.K. Dipojono, F. Rusydi, A theoretical study of monodeuteriation effect on the rearrangement of trans-HCOH to H_2CO via quantum tunneling with dft and wkb approximation, Proc. Eng. 170 (2017) 119–123.
[41] R.N. Fadilla, N.D. Aisyah, H.K. Dipojono, F. Rusydi, The first-principles study on the stability of trans-hcoh in various solvents, J. Phys. Conf. Ser. 853 (2017) 012031.
[42] A. Fortunnelli, J. Tomasi, The implementation of density functional theory within the polarizable continuum model for solvation, Chem. Phys. Lett. 231 (1994) 34–39.
[43] E.D. Glendening, A.E. Reed, J.E. Carpenter, F. Weinhold, NBO Version 3.1.
[44] D.A. McQuarrie, J.D. Simon, Physical Chemistry - A Molecular Approach, University Science Books, 1997.
[45] D.L. Lide, in: W.M. Haynes (Ed.), CRC Handbook of Chemistry and Physics, 96th ed., CRC Press/Taylor and Francis, Boca Raton FL, USA, 2015, pp. 9–48.
[46] K. Kuchitsu (Ed.), Structure of Free Polyatomic Molecules – Basic Data, Springer, Heidelberg NY, USA, 1998.